Received: 3 September 2019 | Revised: 19 November 2019 | Accepted: 22 November 2019

DOI: 10.1111/gcb.14950

PRIMARY RESEARCH ARTICLE

Global Change Biology WILEY

Higher than expected CO_2 fertilization inferred from leaf to global observations

Vanessa Haverd[1] | Benjamin Smith[1,2,3] | Josep G. Canadell[1] | Matthias Cuntz[4] | Sara Mikaloff-Fletcher[5] | Graham Farquhar[6] | William Woodgate[7] | Peter R. Briggs[1] | Cathy M. Trudinger[8]

[1]CSIRO Oceans and Atmosphere, Canberra, ACT, Australia

[2]Department of Physical Geography and Ecosystem Science, Lund University, Lund, Sweden

[3]Hawkesbury Institute for the Environment, Western Sydney University, Penrith, NSW, Australia

[4]AgroParisTech, Université de Lorraine, INRA, UMR Silva, Nancy, France

[5]National Institute of Water and Atmospheric Research, Wellington, New Zealand

[6]Research School of Biology, The Australian National University, Canberra, ACT, Australia

[7]CSIRO Land & Water, Canberra, ACT, Australia

[8]CSIRO Oceans and Atmosphere, Melbourne, Vic., Australia

Correspondence
Vanessa Haverd, CSIRO Oceans & Atmosphere, GPO Box 1700, Canberra, ACT 2601, Australia.
Email: vanessa.haverd@csiro.au

Funding information
Australian Government's National Environmental Science Program; Strategic Research Area MERGE; CSIRO Distinguished Visiting Scientist; French National Research Agency, Grant/Award Number: ANR-11-LABX-0002-01; NIWA

Abstract

Several lines of evidence point to an increase in the activity of the terrestrial biosphere over recent decades, impacting the global net land carbon sink (NLS) and its control on the growth of atmospheric carbon dioxide (c_a). Global terrestrial gross primary production (GPP)—the rate of carbon fixation by photosynthesis—is estimated to have risen by (31 ± 5)% since 1900, but the relative contributions of different putative drivers to this increase are not well known. Here we identify the rising atmospheric CO_2 concentration as the dominant driver. We reconcile leaf-level and global atmospheric constraints on trends in modeled biospheric activity to reveal a global CO_2 fertilization effect on photosynthesis of 30% since 1900, or 47% for a doubling of c_a above the pre-industrial level. Our historic value is nearly twice as high as current estimates (17 ± 4)% that do not use the full range of available constraints. Consequently, under a future low-emission scenario, we project a land carbon sink (174 PgC, 2006–2099) that is 57 PgC larger than if a lower CO_2 fertilization effect comparable with current estimates is assumed. These findings suggest a larger beneficial role of the land carbon sink in modulating future excess anthropogenic CO_2 consistent with the target of the Paris Agreement to stay below 2°C warming, and underscore the importance of preserving terrestrial carbon sinks.

KEYWORDS

amplitude of seasonal cycle, carbonyl sulfide, CO_2 fertilization, coordination of photosynthesis, gross primary production, land carbon sink

1 | INTRODUCTION

Four independent lines of evidence indicate intensifying terrestrial biosphere activity (Campbell et al., 2017; Forzieri, Alkama, Miralles, & Cescatti, 2017; Graven et al., 2013; Le Quéré et al., 2018), namely the increasing positive trends in (a) the global net land carbon sink (NLS; Jinfeng et al., 2017; Le Quéré et al., 2018; Li et al., 2018); (b) the amplitude of the seasonal cycle (ASC)

of atmospheric CO_2 (c_a) in the Northern Hemisphere (Forkel et al., 2016; Graven et al., 2013; Thomas et al., 2016); (c) satellite-observed leaf area (Forzieri et al., 2017; Zhu et al., 2016); and (d) global gross primary production (GPP), as inferred from long-term atmospheric carbonyl sulfide concentration (COS) records (Campbell et al., 2017). Attribution and future projection of these trends relies on terrestrial biosphere models (TBMs) that encapsulate mechanistic understanding of the terrestrial carbon cycle and are used to inform the global carbon budget (Le Quéré et al., 2018; Sitch et al., 2015).

Our focus in this work is on the historical increase in global GPP. The estimate presented by Campbell et al. (2017) [(31 ± 5)% increase (2σ, 1900–2010)] is based on the long-term atmospheric carbonyl sulfide (COS) records, derived from ice-core, firn and ambient air samples. Campbell et al. (2017) interpreted these records using a model that simulates the changes in atmospheric COS concentration according to the changes in its sources and sinks—including a large sink that is related to GPP—and suggested that their results provide a global-scale benchmark for historical carbon cycle simulations. The accuracy of COS-based GPP estimates depends in part on accounting for different environmental responses of COS and CO_2 uptake (Whelan et al., 2018). Despite recent progress in accounting for these different responses (Kooijmans et al., 2019), the estimate by Campbell et al. (2017) remains the only COS-based estimate of the historical change in global GPP and has yet to be utilized as a benchmark for global TBMs. Previous estimates of the global GPP increase over this timescale are restricted to process model simulations that suggest a much lower increase of 16 ± 4% (Keenan et al., 2016). While there is consensus that the simulated increase is largely driven by CO_2 fertilization (Baldocchi, Ryu, & Keenan, 2016; Keenan et al., 2016; Schimel, Stephens, & Fisher, 2015), the general underprediction of the global GPP increase means that a large fraction (>one-third) of the 31% ± 5% growth is unaccounted for by current TBMs, impacting their future projections of the dynamics of the NLS. Furthermore, it remains to be explored whether the large COS-based increase in global GPP is compatible with the other lines of evidence for increased terrestrial biospheric activity, particularly trends in the NLS and ASC.

The NLS may be estimated as the sum of atmosphere and ocean sinks minus the emissions from cement productions and combustion of fossil fuels. The NLS is positive (2.3 ± 0.4 PgC/year; 2007–2016) and has been increasing at a rate of 0.061 ± 0.02 (1 *SE*) PgC/year^2 (1980–2016; Le Quéré et al., 2018), implying that, globally, GPP is in excess of ecosystem carbon loss by fire and respiration, and that GPP is increasing faster than ecosystem carbon loss. As such, the magnitude and trend in the NLS provide indirect constraints on the magnitude of global GPP increase. Interannual variations in the NLS—driven largely by anomalies in plant productivity (Ahlström et al., 2015)—also provide a constraint on the sensitivity of simulated productivity to temperature and precipitation anomalies (Piao et al., 2013).

The ASC in the Northern Hemisphere (averaged over latitudes >45°N, 500 mb), as calculated from aircraft data in two separate 3- to 4-year periods (IGY data; 1958–1961; Keeling, Harris, & Wilkins, 1968) and (HIPPO and NOAA data; 2009–2011; Wofsy, 2011), has been reported to show a large increase of (57 ± 7)% (Graven et al., 2013). Atmospheric transport simulations reveal that these ASC observations are sensitive to net uptake on land north of 40°N, with negligible contributions from lower latitudes or from the ocean (Graven et al., 2013). The increase in ASC in studies examining the multi-model TBM simulations combined with atmospheric transport modeling show that the simulated increase in seasonal amplitude of c_a is generally underpredicted both at high altitude (Graven et al., 2013) and at remote surface stations (Thomas et al., 2016). It has been speculated that this is because TBMs underpredict CO_2 and/or warming effects on GPP (Forkel et al., 2016; Thomas et al., 2016), but changes in the seasonal cycle of ecosystem respiration (e.g., Liptak, Keppel-Aleks, & Lindsay, 2017), including winter respiration (Parazoo et al., 2016), must also be implicated.

The magnitude of the CO_2 fertilization effect on photosynthesis depends on biochemical demand for CO_2 and supply of CO_2 from the atmosphere to the chloroplast via the stomata. Global TBMs typically simulate biochemical demand by C_3 plants (accounting for ~77% of photosynthesis globally; Still, Berry, Collatz, & Defries, 2003) using the photosynthesis model of Farquhar and von Caemmerer (1981), which equates gross assimilation (A) with the lesser of Rubisco and electron transport-limited assimilation rates (A_c and A_j, respectively). The sensitivities of A_c and A_j to c_a are well known (Lloyd & Farquhar, 1996; Long, 1991) and quite different, meaning that the relative contributions of A_c (high sensitivity) and A_j (low sensitivity)-limited rates to A_n are an important determinant of the leaf-level CO_2 fertilization effect. At the leaf level, the dimensionless elasticity of gross carbon assimilation by photosynthesis (A) to c_a $\left(\beta = \frac{\partial A}{\partial c_a}\frac{c_a}{A}\right)$ characterizes the instantaneous sensitivity of A to c_a. Leaf gas-exchange observations (Farquhar & von Caemmerer, 1981; Maire et al., 2012) support the coordination theory (Chen, Reynolds, Harley, & Tenhunen, 1993; Farquhar & von Caemmerer, 1981; Wang et al., 2017) that plants optimize the productivity in their environment through relative nitrogen investment in electron transport and Rubisco-limited steps in the photosynthesis chain, such that they are co-limiting. Such co-limitation occurs for average growing conditions spanning wide-ranging c_a, vapor pressure deficit, light, and temperature (Maire et al., 2012), with the result that the long-term contributions of A_c and A_j to A are approximately equal. The results of Maire et al. (2012; reproduced in Figure 1a) represent the predictions of A_c and A_j for mean growth conditions of the previous month, based on the experimental values of photosynthetic leaf traits. The response to increasing c_a appears to be most marked, with a reduction in Rubisco content of leaves, in plants growing in nutrient-limited environments (Wong, 1979). This coordination of photosynthesis, and its associated constraint on β, is not generally represented in TBMs, although approaches are emerging that enable such representation (Ali et al., 2016; Haverd et al., 2018; Wang et al., 2017). The usefulness of this constraint on CO_2 fertilization as a driver of global GPP variation has so far been largely neglected.

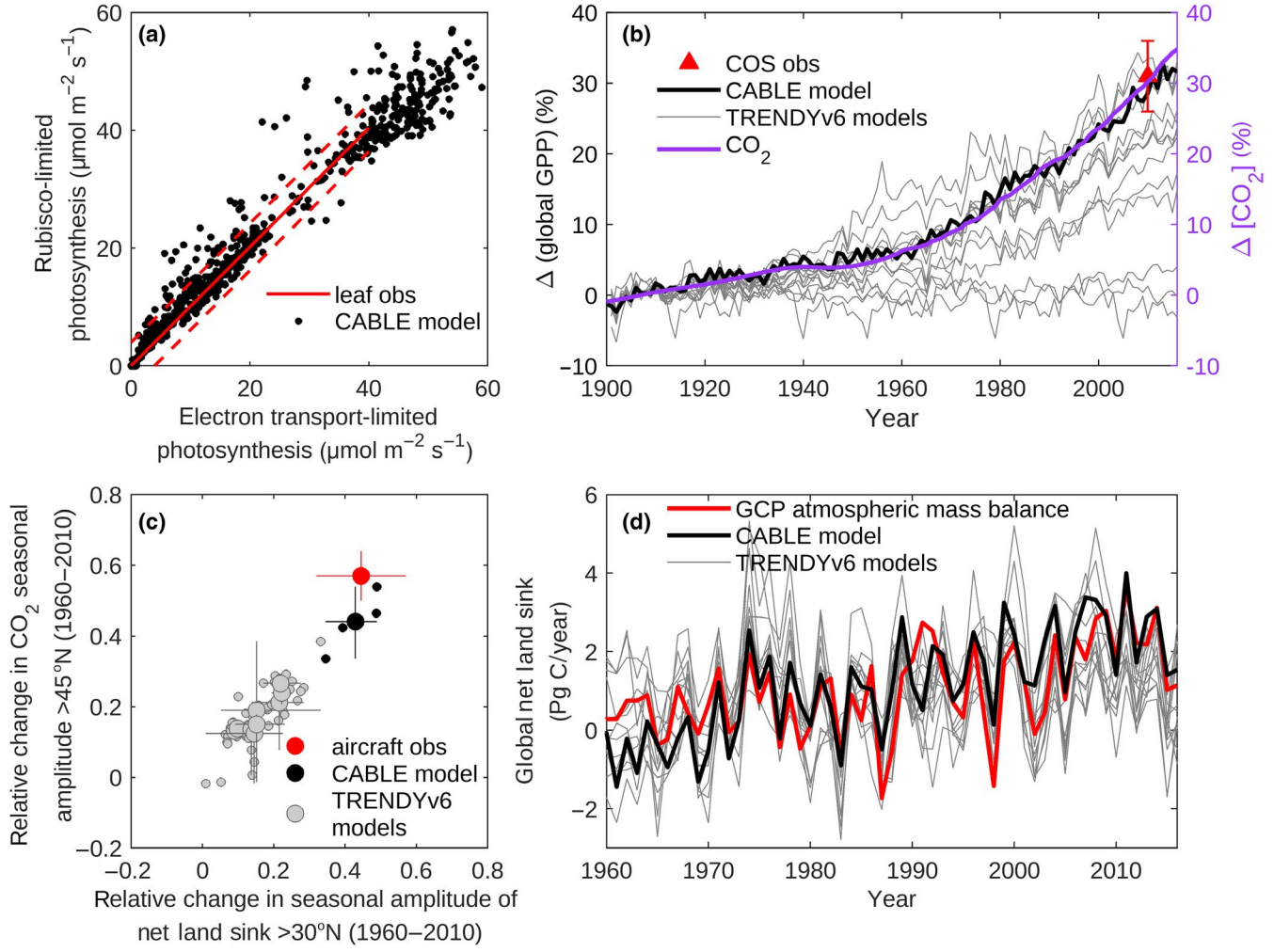

FIGURE 1 Constraints on trends in global-scale terrestrial biospheric activity. (a) Coordination of photosynthesis. Black: CABLE predictions of A_c versus A_j contributions to C_3 photosynthesis (1980–2015) at 1,000 randomly distributed grid cells across the global ice-free land surface. Red lines reproduced from Maire et al. (2012): A_c versus A_j under average plant growth conditions predicted from observed leaf-level traits (solid); predictive error (dashed). (b) Increase in global gross primary production relative to 1900, simulated by CABLE (black) and TRENDYv6 (Le Quéré et al., 2018; Sitch et al., 2015 grey), and inferred from observations of [COS] (4) (red); Increase in c_a (purple; Dlugokencky & Tans, 2017). (c) Increase in amplitude of the seasonal cycle (ASC) of c_a (1958–1961 to 2009–2011, >45°N, 500 mb) versus ASC of net land carbon sink (NLS) north of 30°N: aircraft observations (Keeling et al., 1968; Wofsy, 2011) and corresponding TM3 (Heimann & Körner, 2005) atmospheric inversion reproduced from Graven et al. (2013; red); CABLE-TM3 (black); TRENDYv6-TM3 (grey); average for each model (large circles); individual ensemble members (small circles); ensemble range (bars; Section 2). (d) Time-series of annual global NLS: CABLE (black); TRENDYv6 (grey); Global Carbon Project (GCP) mass balance estimate (note 0.4 PgC/year uncertainty), as the sum of atmosphere and ocean sinks, minus fossil fuel emissions (red). Linear trends (1980–2015): 0.061 ± 0.02 (1 *SE*) PgC/year^2 (GCP) and 0.067 ± 0.01 PgC/year^2 (CABLE). See also Figure S1 for metrics related to the NLS

Here we reconcile the leaf-level constraint on the CO_2 fertilization effect imposed by coordination of photosynthesis with the constraints implied by trends in biospheric activity reflected in globally observed increases in ASC, NLS, and GPP inferred from atmospheric COS. This is achieved using mechanistic principles encapsulated by a TBM framework (Pugh et al., 2016) that links biophysics, ecophysiology, biogeochemistry (including nitrogen cycle), and vegetation structural dynamics via dependencies on climate, c_a, disturbance and land-use drivers, and evolving system state. We quantify the contribution of the biospheric CO_2 response to the trend in global GPP and explore the potential implications for the future evolution of the NLS.

2 | MATERIALS AND METHODS

2.1 | Community Atmosphere-Biosphere Land Exchange

The Community Atmosphere-Biosphere Land Exchange model (CABLE) is a biogeochemical land surface model (including N-cycle) that represents vegetation structural dynamics. CABLE consists of a biophysics core (Haverd, Cuntz, Nieradzik, & Harman, 2016; Kowalczyk et al., 2013; Wang et al., 2011), the CASA-CNP biogeochemistry module (Wang, Law, & Pak, 2010), the POP module for woody demography and disturbance-mediated landscape

heterogeneity (Haverd, Smith, et al., 2013), and a module for land use and land management (POPLUC; Haverd et al., 2018). The land use and land cover change module is driven by gross land use transitions and wood harvest area. CABLE is one of an ensemble of ecosystem and land surface models contributing to the Global Carbon Project's annual update of the global carbon budget (Le Quéré et al., 2018) via the TRENDY ensemble.

This article uses a version of CABLE that was recently extended to account for (a) tree demography and disturbance-mediated landscape heterogeneity; (b) land use and land cover change; and (c) coordinated leaf nitrogen investment in electron transport and Rubisco-limited steps in the photosynthesis chain, such that they adjust seasonally and across biomes to be co-limiting (Haverd et al., 2018). This version also includes a new diagnostic elasticity $\beta = (\partial A/\partial c_s)\,(c_s/A)$ that allows the GPP increase attributable to the leaf-level component of the CO_2 fertilization effect to be isolated as $(\partial A/\partial c_s)\,\Delta c_s$, where c_s is the CO_2 concentration at the leaf surface.

2.2 | CABLE: Coordination of C_3 photosynthesis

CABLE represents the coordination of C_3 photosynthesis, adjusting electron transport and Rubisco-limited rates (Farquhar, Caemmerer, & Berry, 1980) to be co-limiting (Haverd et al., 2018). This is achieved by dynamically optimizing the ratio b_{JV} of the maximum rate of electron transport (J_{max}) to the Rubisco-catalyzed maximum rate of carboxylation (V_{cmax}) at standard temperature. The optimization aims to maximize the rate of photosynthesis per unit leaf nitrogen. The approach to optimization of b_{JV} is based on the following three assumptions:

1. Leaf nitrogen resources may be dynamically redistributed at a 5-day timescale at no cost, that is b_{JV} is optimized, such that net photosynthesis (given total available leaf nitrogen) accumulated over the last 5 days (approximately the timescale for turnover of photosynthetic nitrogen; Thornley, 2004) would have been maximized.
2. Leaf nitrogen resources available for partitioning between Rubisco and electron transport capacity are proportional to effective nitrogen content (N_{eff}), defined as the sum of prior estimates of $V_{cmax,0}$ and $J_{cmax,0}$, weighted by relative cost factor $c_{cost,JV}$. (There are no explicit nitrogen pools corresponding to Rubisco and electron transport capacities because there are no explicit nitrogen pools in the photosynthesis model of Farquhar et al. 1980.)
3. The prior values of $V_{cmax,0}$ (related to time-varying prognostic leaf nitrogen content) and b_{JV} are prescribed according to the synthesis of globally distributed leaf gas-exchange measurements by Walker et al. (2014).

The method for implementing these assumptions in CABLE is:

1. Maintain a 5-day history of sub-diurnal leaf-level meteorology (absorbed PAR; leaf-air vapor pressure difference; leaf temperature, CO_2 concentration at the leaf surface) for sunlit and shaded leaves, such that total photosynthesis over the last 5 days can be reconstructed.
2. Construct a function that calculates leaf nitrogen cost per unit net photosynthesis. Inputs to this function are as follows: (a) current estimate of b_{JV}, (b) effective leaf nitrogen content (related to prior value of $V_{cmax,0}$), (c) 5-day history of sub-diurnal leaf-level meteorology.
3. At the end of each day, solve for b_{JV} that maximizes the total photosynthesis over the last 5 days per unit effective leaf nitrogen, and update $V_{c,max,0}$ and $J_{max,0}$ values.

The emerging contributions of electron transport and Rubisco-limited rates contribute approximately equally to total net photosynthesis.

2.3 | Ensemble of current TBMs

We use simulations from the TRENDYv6 ensemble of TBMs to represent current TBMs: these models (Table S1) encapsulate mechanistic understanding of the terrestrial carbon cycle and are used to inform the global carbon budget. Simulations generated using common protocols and forcings are made available at monthly time resolution and variable spatial resolution for the time period 1860–2016. We used estimates of the simulated annual global NLS (Figure 1d) directly from the Global Carbon Budget 2017 (42). Gridded TRENDY outputs (GPP and NLS) were downloaded from sftp://trendy-v6:gcp-2017@emps-cpdn.ex.ac.uk/output/ (accessed September 21, 2017).

2.4 | CABLE: Historic simulations

Global simulations were performed at 0.5 × 0.5° spatial resolution, with time steps of 3 hr (biophysics); 1 day (biogeochemistry); and 1 year (woody demography, disturbance, land use change). The nitrogen cycle was enabled, but not the phosphorus cycle. Recently developed parameterizations for drought response of stomatal conductance and effects of leaf litter on soil evaporation were enabled (Haverd et al., 2016). The relationship between $V_{c,max,0}$ and leaf nutrient status was prescribed using the meta-analysis of globally distributed leaf gas-exchange data by Walker et al. (2014). Other photosynthetic parameters were prescribed to be consistent with this analysis, in which any effect of mesophyll conductance (g_m) is implicit in the inferred, effective value of $V_{cmax,0}$. This effective value will be lower than the true Rubisco capacity owing to the resistance to gas transport between the stomatal chamber and the chloroplast stroma where carboxylation takes place. Following the recent recommendation of Bahar, Hayes, Scafaro, Atkin, and Evans (2018): "while incorporating g_m into models to estimate GPP is theoretically appealing, in practice it is not yet possible as it requires knowledge of Rubisco kinetic parameters for a range of evergreen tree species, an estimate of g_m and its

temperature response for representative species," we chose not to account for g_m explicitly.

Simulations were driven by (a) daily CRU-NCEP V7 (1901–2016; Viovy, 2009), down-scaled to 3-hourly resolution using a weather generator (Haverd, Raupach, et al., 2013); (b) CO_2 (1-year) resolution (Dlugokencky & Tans, 2017); (c) gridded nitrogen deposition (10-year resolution; Lamarque et al., 2011); and (d) gridded gross land use transitions and harvest (1500–2015) and initial land use states (1,500) from the LUH2 harmonized land use data set (Hurtt et al., 2011; Hurtt, Chini, Frolking, & Sahajpal, 2016).

The "Excl. Coord." configuration of the model that excluded the coordination of C_3 photosynthesis differed from the full model in three ways: (a) dynamic optimization of the $J_{max,0}/V_{cmax,0}$ ratio was disabled; (b) the $J_{max,0}/V_{cmax,0}$ ratio was set to a low value of 1.3 to ensure that A_J was always less than A_c; (c) $V_{cmax,0}$ was scaled up by a factor of 1.25 to ensure that the simulated present day GPP from this configuration and the full model configuration are approximately equal (Figure S3a).

The partitioning of CABLE's historic global GPP between climate and CO_2 effects (Figure 2a; Figure S5) was achieved by subtracting the results of a "CO_2 only experiment" from an "all driver experiment." In the CO_2-only experiment, CO_2 and land use are varied and recycled meteorology (1901–1930) is prescribed.

In contrast, the CO_2-driven increase in GPP is derived using the "S1" scenario from the TRENDY protocol, in which fixed 1,860 land cover is assumed and only CO_2 is varied. This additional simulation allows for direct comparison of the simulated CO_2 fertilization effect with the TRENDYv6 ensemble.

We performed further single and double-factorial experiments to isolate the effects of single drivers and driver combinations: c_a only; temperature only; c_a and temperature together; precipitation; land use change.

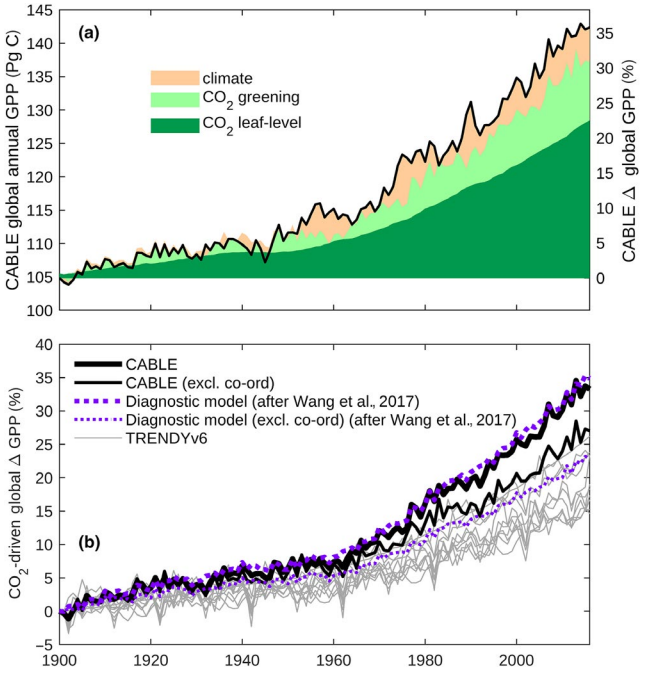

FIGURE 2 CO_2 fertilization effect on global gross primary production (GPP). (a) Full CABLE simulation with dynamic land use (solid black lines) attributed to: (i) climate effect and c_a × climate interaction effect (orange); (ii) CO_2 greening effect (light green); (iii) CO_2 leaf-level effect (dark green). (b) CO_2-driven increase in global GPP relative to 1900 (fixed 1,860 land use), as simulated by: (i) full CABLE (thick black line); (ii) CABLE without coordination of photosynthesis, that is assimilation is always limited by electron transport (thin black line); (iii) the TRENDYv6 ensemble (grey lines) and (iv) full diagnostic photosynthesis algorithm of Wang et al. (2017), applied using prescribed vegetation cover from CABLE (thick purple dashed line); (v) diagnostic photosynthesis algorithm of Wang et al. (2017) without coordination (i.e., assimilation is always limited by electron transport), applied using prescribed vegetation cover from CABLE (thin purple-dashed line)

2.5 | CABLE: Future projections

The Representative Concentration Pathways (RCPs) were designed to inform the mitigation and adaptation policies, and describe different climate futures based on a range of emissions scenarios (van Vuuren et al., 2011). The Shared Socioeconomic Pathways (SSPs) consist of trajectories of future human development with different socioeconomic conditions and associated land use projections (O'Neill et al., 2017). The SSPs can be combined with the RCPs to explore a range of futures for climate change and land use change. We used SSP1 combined with RCP2.6 (low conversion of land use and low emissions) to project the NLS to 2006–2099 (Figure 5). This simulation was forced using harmonized historic and future data sets for climate (IPSL-CM5A-LR from ISI-MIP2a; Warszawski et al., 2014; https://esg.pik-potsdam.de/search/isimip2a/, accessed December 19, 2017), land use (Hurtt et al., 2016; Hurtt, Chini, Frolking, & Sahajpal, 2018), CO_2 (van Vuuren et al., 2011), and nitrogen deposition (Lamarque et al., 2011). We performed two simulations: (a) full simulation with all drivers varying to give the NLS and (b) a simulation of the biophysical sink (i.e., the net carbon uptake driven by changing climate, CO_2, and nitrogen deposition) for each land cover class, with class contributions weighted by their time-varying area fractions.

To assess the CO_2 fertilization effect on GPP for a doubling of c_a, we also performed a projection (2006–2099) using CO_2 forcing from RCP8.5, combined with fixed IPSL-CM5A-LR climate (repeated 1990–2010) and land cover (2015). The simulated trend in GPP over this period corresponds to projected CO_2 fertilization effects of (47 ± 2)% for a doubling of c_a (300–600 ppm, constant climate and land use) for the globe and (42 ± 2)%, for the Northern Hemisphere extra-tropics >30°N.

2.5.1 | Amplitude of CO_2 seasonal cycle in the Northern Hemisphere

The increase in amplitude of seasonal cycle in c_a was simulated by using air–land fluxes from the CABLE and TRENDYv6 TBMs as

boundary conditions for "fine grid" version of the global atmospheric tracer transport model TM3 (Heimann & Körner, 2005), with an approximate horizontal resolution of 3.8 × 5° and 19 vertical levels. It was driven by winds from NCEP reanalysis (Kalnay et al., 1996). Influences from outside of the terrestrial biosphere on seasonal CO_2 amplitude in the NH, including fossil fuel emissions and air–ocean fluxes have been shown to be negligible (Graven et al., 2013), and were omitted in this analysis. The simulated monthly time series corresponding to each 3- to 4-year aircraft campaigns was interpolated to the 500 mb isobar and linearly detrended. The seasonal CO_2 amplitude was quantified by taking the difference of the maximum and minimum monthly detrended concentrations.

The NLS in the Northern Hemisphere is the net sum of two similarly large flux components (GPP and ecosytem carbon loss—largely ecosystem respiration, but also including fire loss—to the atmosphere: $R'_{eco} = GPP - NLS$) which both have summer seasonal peaks. Poor predictions of the ASC magnitude may result from small errors in the relative phase and/or the amplitude of either flux, which in turn may influence the simulated ASC trends. To address this source of uncertainty, we made the assumption that the seasonal amplitude in GPP is well-simulated (as confirmed by comparison with latitudinally averaged upscaled FluxNET data (Jung et al., 2011)), but that the relative phase of R'_{eco} may vary by ±14 days and the amplitude by ±20% compared with the simulated values. Such errors in the phase and amplitude of simulated R'_{eco} may arise from a number of factors such as: (a) approximating soil carbon stocks as pools with discrete turnover times and associated effective soil depths (Koven et al., 2013), (b) neglecting seasonal acclimation effects on autotrophic and heterotrophic respiration. Under this assumption, we constructed 25 ensembles of monthly gridded NLS for CABLE and for each model of the TRENDYv6 ensemble for which monthly output could be obtained. Each ensemble member corresponded to one of five equally spaced phase shifts and amplitude scalings of R'_{eco}, while conserving the total annual flux. The ensembles were then used to generate 25 estimates of monthly c_a for Point Barrow (*BRW* 71.3°N, 156.6°W) and Cape Kumukahi (KMK, 19.5°N, 155.6°W), marine boundary layer stations examined by Wenzel, Cox, Eyring, and Friedlingstein (2016). Observed monthly mean in situ atmospheric CO_2 concentrations at BRW and KMK were obtained from the Scripps Institute of Oceanography records (http://scrippsco2.ucsd.edu/data/atmospheric_co2; Keeling et al., 2001). The ensemble members corresponding to each TBM were selected such that perturbed ASC (2010) at both stations matched the actual ASC to within ±3 ppm. These selected subsets were then used as input to TM3 to simulate the relative change in ASC, with mean and uncertainties for each model expressed as the mean and range of ensemble members (Figure 1c).

3 | RESULTS

Using the CABLE TBM, enabled to represent the coordination of photosynthesis (Haverd et al., 2018; Figure 1a), we successfully capture four major independent global-scale benchmarks of trends in biospheric activity. They are as follows: (a) multi-decadal increases in global GPP (Figure 1b), (b) amplitude of the seasonal CO_2 cycle in the Northern Hemisphere (Figure 1c), (c) global NLS (Figure 1d) including its mean, trend, and interannual variations that are considered a proxy for tropical temperature sensitivity (Figure S1), and (d) leaf area index (Figure S2). Using model experiments to attribute the effects of changing climate and c_a (Section 2), we find that the total increase in GPP is predominantly driven by CO_2 (Figure 2a). The remaining climate-driven component (14% of the full increase, Figure 2a) is largely attributable to warming and (temperature × c_a) interactions in Northern Hemisphere extratropical ecosystems (Figure 3c; Figure S5).

We estimate a historic global CO_2 fertilization effect on photosynthesis of 30% (1900–2010; 296–389 ppm c_a) that is significantly higher than current TBM (TRENDYv6) estimates (17 ± 4%; 1σ), Figure 2b. We project a GPP increase of (47 ± 2)% for a doubling

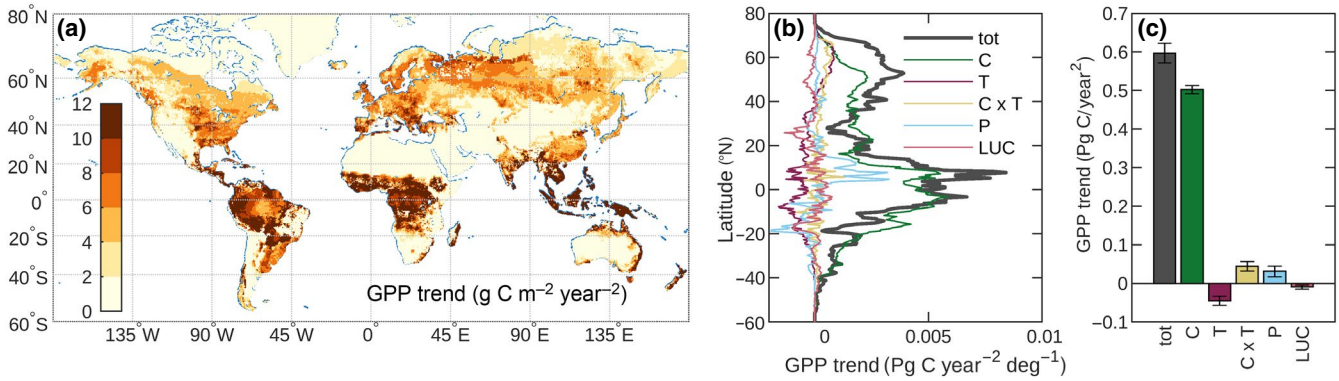

FIGURE 3 Spatial and driver attribution of gross primary production (GPP) trend (1980–2016). (a) Spatial distribution. (b) Latitudinal distribution of driver components. (c) Driver attribution of global GPP trend. Driver attribution is achieved by factorial experiments in which only one or a pair of drivers is varied while all others are fixed (Section 2). Tot = total effect; C = c_a only; T = temperature; C × T = c_a–temperature interaction; P = precipitation; LUC = land use change. Only major drivers are isolated. Additional drivers (nitrogen deposition; specific humidity; wind speed; incoming short and longwave radiation) and their interactions are not isolated but may contribute to the total effect. Error bars represent standard errors from linear regression fits to each driver component (Section 2)

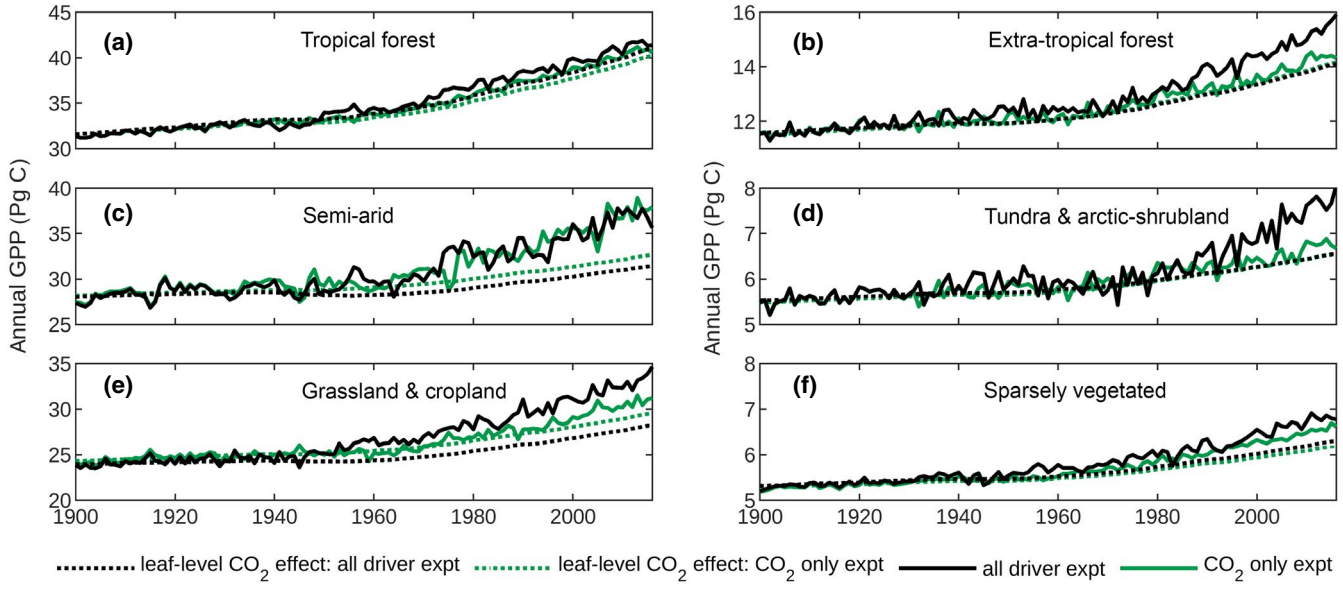

FIGURE 4 CO_2 fertilization effect on gross primary production (GPP) by region. Regions correspond to land cover classification (Figure S3). Solid black line: full CABLE simulation with all drivers varying ("all driver expt"). Dotted black line: leaf-level CO_2 effect as a component of the all driver expt. Solid green line: CABLE simulation in which CO_2 is varying, actual land cover assumed and recycled meteorology (1901–1930) is prescribed ("CO_2 only expt"). Dotted green line: leaf-level CO_2 effect as a component of the CO_2 only experiment. The difference between the green-dotted and solid lines represents the CO_2 greening effect. The difference between the solid green and black line represents the climate effect and c_a × climate interaction effect on GPP

of c_a (300–600 ppm, constant climate and land use, Section 2). Our corresponding extratropical Northern Hemisphere estimate (>30°N) of (42 ± 2)% (1 *SE*) is at the high end of the previously reported estimate (32 ± 9)% (2σ) obtained by constraining an ensemble of climate-carbon cycle model projections with observed trends in the ASC of c_a (Wenzel et al., 2016).

The simulation of coordination of photosynthesis contributes strongly to the high-CO_2 fertilization effect in CABLE (Figure 2b). Both CABLE configurations agree well with present-day GPP estimates based on upscaled eddy flux data (Jung et al., 2011) in terms of magnitude and latitudinal distribution (Figure S3b), highlighting that the contrasting CO_2 elasticities (Figure S3a) lead to different magnitudes and latitudinal distributions of the NLS (Figure S3a,c).

We partition the CO_2 fertilization effect on GPP between leaf-level and greening effects, using the dimensionless β diagnostic, which expresses the instantaneous sensitivity of photosynthesis to CO_2. This allows the contribution of greening (i.e., increased light harvesting capacity due to the investment of additional plant carbon in a higher leaf area) to be calculated as the difference between overall GPP increase and the leaf-level contribution to that increase. We find that 70% of the CO_2-driven increase in global GPP is attributable to the leaf-level effect, that is the CO_2-induced increase in GPP that occurs at constant leaf area. The remaining 30% is attributable to the CO_2-greening effect (Figure 2a), that is the positive feedback resulting from the investment by vegetation of a proportion of increased productivity in enhanced leaf area. The leaf-level effect from rising c_a includes both the direct biochemical effect (effect of c_a on Rubisco carboxylase as a substrate and inhibition of ribulose bisphosphate oxygenation and hence photorespiration; Long, 1991) and the indirect effect of enhanced water-use efficiency resulting from the reductions in stomatal conductance that adjusts to maximize carbon gain with respect to water loss (Franks et al., 2013).

Two-thirds of the global CO_2-greening effect is attributable to semiarid ecosystems. Over the (1982–2010) period, the 16% increase in semiarid GPP may be partitioned between leaf-level (6%) and CO_2-greening (10%) components (C), in agreement with the 11% increase in foliage cover reported for the same period in warm semiarid regions where relative change in foliage cover may be equated with the CO_2-greening effect on GPP (Donohue, Roderick, Mcvicar, & Farquhar, 2013). In contrast, the tropical forest GPP (1982–2010) increases proportionately with c_a (both 12%), almost entirely because of the leaf-level effect (Figure 4a), in agreement with the increase (12%) inferred from tropical forest catchment water balance (Yang, Donohue, Mcvicar, Roderick, & Beck, 2016). Globally, the leaf-level CO_2 effect dominates total GPP increase (Figure 2a), meaning that vegetation greenness trends are not generally a direct proxy for GPP trends (see also De Kauwe, Keenan, Medlyn, Prentice, & Terrer, 2016).

To explore the implications of a higher than expected CO_2 fertilization effect for the future fate of the land carbon sink, we employed CABLE, constrained by observed global trends (Figure 1b–d) to project the net land sink (2006–2099) under a low emissions, moderate land use change scenario (RCP2.6). In this scenario, c_a peaks at 440 ppm in 2050, global mean air temperature stabilizes at 2.4° above the 1900 level by 2040, carbon-climate feedbacks are expected to be small (Ciais, Sabine, & Bala, 2013), and emissions from carbon-stored permafrost are negligible (McGuire et al., 2018). Given these assumptions, we find that the terrestrial biosphere

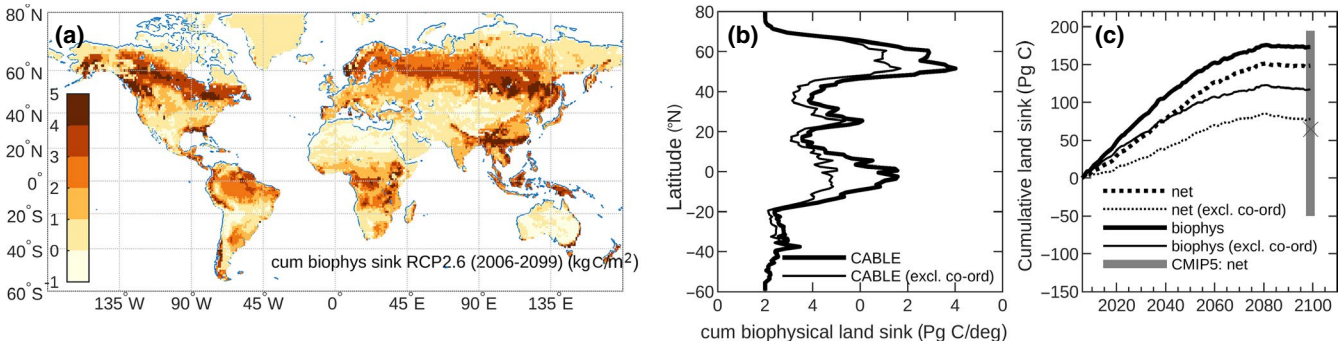

FIGURE 5 Projected cumulative land sink under Representative Concentration Pathway (RCP) 2.6 scenario. (a) Spatial distribution of cumulative biophysical (CO_2 and climate-driven) sink. (b) Latitudinal distribution of cumulative biophysical sink (full CABLE simulation, and with coordination of photosynthesis excluded). (c) Time series of projected (2006–2099) biophysical land sink (solid black lines) and net land sink (dotted black lines) relative to 2006 (full CABLE simulation (thick lines), and with coordination of photosynthesis excluded (thin lines). The range (bar) and average (cross) cumulative net land carbon sink projected by the CMIP5 carbon-climate models (Ciais et al., 2013) are shown in grey

would continue to sequester carbon well into the second half of the century, leading to a cumulative net land sink (CO_2, climate, and land use change driven) of 149 PgC by the end of the century, significantly larger than the mean of the CMIP5 carbon-climate model ensemble under the RCP2.6 scenario (65 PgC; Ciais et al., 2013), but well within the among-model spread of the same ensemble (−50 to +195 PgC; Figure 5c). Adjusting to include only biophysical effects (CO_2 and climate-driven sink), we estimate a cumulative biophysical sink of 174 PgC (spatial distribution; Figure 5a,b), equivalent to 17 years of anthropogenic CO_2 emissions at current rates. This sink is large compared to the potential carbon uptake attainable by the recovery of existing secondary forests (117 Pg; Houghton & Nassikas, 2018), and 57 PgC larger than if a lower CO_2 fertilization effect (simulated by CABLE disregarding coordination) is assumed (Figure 4c).

4 | DISCUSSION

The magnitude of the simulated CO_2 effect on electron transport-limited photosynthesis (A_j), the increase above this effect due to coordination, and the simulated reduction in β with c_a emerging from our study are supported by other evidence. First, the historical CO_2 fertilization effect on global GPP that is predicted by CABLE Excl. Coord. (A limited by A_j) is comparable to that predicted by the diagnostic photosynthesis algorithm of Wang et al. (2017) that is unconstrained by coordination theory, and explicitly equates A with A_j (Figure 2b). Furthermore, the same algorithm predicts a decline of β of (37%→19%) for a doubling of c_a (400→800 ppm) at 25°C (Keenan et al., 2016). Using CABLE Excl. Coord., we find similar corresponding sensitivities (35%→17%), but much higher values of β (56%→34%) for full CABLE, in which coordination is allowed to occur (see also Figure S3a for latitudinal profiles of β at different c_a). Second, by applying the full diagnostic photosynthesis algorithm of Wang et al. (2017) that is constrained by their alternate implementation of coordination theory, we confirm a large increase in c_a sensitivity of historic global GPP when coordination is simulated, compared with the simulations in which A is limited to A_j (Figure 2b). Third, as noted above, β decreases as c_a increases, and this is due in part to a decline in maximum carboxylation capacity (V_{cmax}) as relative investment of leaf nitrogen in electron transport increases such that coordination of photosynthesis is maintained. The simulated reduction in V_{cmax} agrees well with CO_2-acclimation effects on V_{cmax} inferred from free-air CO_2 enrichment (FACE) studies (~10% reduction for an increase in c_a from 366 ppm to 567 ppm; Ainsworth & Rogers, 2007). We simulate a decrease of V_{cmax}/J_{max} of around 20% (400–600 ppm c_a), whereas a synthesis of FACE results reports a decrease of only 5% (Ainsworth & Rogers, 2007). The robustness of this average estimate is however questionable, since it relies on a fixed linear relationship between J_{max} and V_{cmax} (Ainsworth & Rogers, 2007). In fact, the proportionality between these quantities probably depends on nutrient status; as Wong (1979) first showed, cotton plants grown under low N (0.6 mmol/L nutrient solution) show a larger reduction of initial slope (V_{cmax}) than do plants grown with plentiful N (24 mmol/L), but even in the latter case V_{cmax}/J_{max} appears to decrease with elevated c_a.

Fourth, our simulated CO_2 responses of GPP and net primary production (NPP; plant growth) in temperate forests globally agree well with the syntheses of data from FACE studies in temperate forests (Ainsworth & Rogers, 2007; Norby et al., 2005; Figure 6). EucFACE provides an exceptional example: here there is a negligible response of aboveground plant growth, probably because of strong phosphorus limitation (Ellsworth et al., 2017). Ecosystem models broadly reproduce the response of ecosystem NPP to elevated CO_2 that is determined experimentally at FACE sites (Hickler et al., 2008; Zaehle et al. 2014). Differences in CO_2 response between CABLE and other ecosystem models are mainly apparent in latitudes south of 15°N (tropics and savanna regions; see Figure S9, showing latitudinal contributions to each TRENDY model's global change in GPP since 1901). Hickler et al. (2008) likewise noted higher simulated responses of NPP to CO_2 in the tropics than seen in temperate forest FACE sites.

Three other models in the TRENDYv6 ensemble simulate a centennial increase (1901–2010) of global GPP of ~30%, similar to

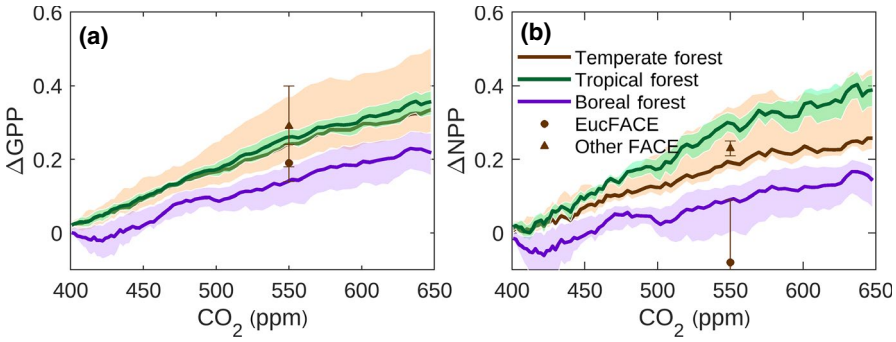

FIGURE 6 CO_2 fertilization effect on gross primary production (GPP; a) and net primary production (NPP; b). The solid lines represent the median predictions of CABLE (fixed land use and climate, rising CO_2 following the trajectory of RCP8.5) for each of temperate, tropical and boreal forests, referenced to a 400 ppm baseline. Shading represents 25th and 75th percentiles. Data points (triangles) are taken from meta-analyses by Ainsworth and Rogers (2007; mean GPP response and standard error: results from two FACE experiments) and Norby et al. (2005; median NPP response and standard error: results from four FACE experiments). These experiments used average baseline and elevated concentrations of CO_2 of 376 ppm and 550 ppm, respectively. Data points (circles) are taken from analysis of the EucFACE experiment by Ellsworth et al. (2017; baseline CO_2: 400 ppm; elevated CO_2 550 ppm). In contrast to "Other FACE", the EucFACE points refer to net (not gross) photosynthesis and aboveground (not total) NPP

that of CABLE and in agreement with the COS observation-based estimate. These provide an opportunity to explore the alternative hypotheses to a higher-than-expected CO_2 fertilization effect as explanations for the high increase in global GPP: (a) LPJ-GUESS simulates very high land use change-induced increase in Northern Hemisphere extratropical GPP (30–60°N), (b) JSBACH and JULES simulate high-land use change and climate-induced increases in GPP in the (−12 to −30°S) latitude band (Figure S9C-D). Land use change is unlikely to induce the increases in GPP in this latitude band because agricultural land area over the last century has been dominated by clearing of tropical forest—a land use conversion that is expected to contribute negatively to trends in NPP (Nyawira, Nabel, Don, Brovkin, & Pongratz, 2016, table 4), and hence GPP. Climate-induced increases in GPP simulated by JULES and JSBACH also appear to be unrealistic, based on apparent temperature and precipitation sensitivities derived from interannual variations in the global NLS (Figure S1b,c), which are known to be dominated by interannual variations in plant productivity in tropical forest and savanna regions (Ahlström et al., 2015). In particular, the apparent temperature sensitivity of JSBACH is positive whereas the atmospheric CO_2 anomalies point to a negative relationship with the temperature (Figure S1b), while JULES exhibits an exaggerated sensitivity to the precipitation (Figure S1c). Thus, the high GPP increases in these models appear to stem partly from simulated climate sensitivities that are too high. Furthermore, the high-relative changes are confounded with significant overestimates of GPP in these same latitude bands, compared with the observation-based FLUXNET estimate (Figure S9a). This suggests that the contributions of land use change and climate alone in other models simulating a large GPP increase are likely to be too high. Our hypothesis of a large CO_2 contribution, particularly in tropical forests and semi-arid regions, is more compatible with the spatial distribution of GPP suggested by the FLUXNET data, and with the hydrological constraints (Yang et al., 2016) on GPP trends in tropical forests, as discussed above. Nonetheless, the role of agricultural expansion and intensification on global greening and GPP remains important and unresolved (Mueller et al., 2014; Zeng et al., 2014).

Our simulated latitudinal and regional distributions of trends in GPP and the NLS (Figure 3a,b; Figures S5–S8) are consistent with the observed increase in the ASC of CO_2 in the Northern Hemisphere (56 ± 10% north of 45°N, 1960–2010; Graven et al., 2013), that is underestimated by current TBMs (Figure 1b), as previously reported (Graven et al., 2013; Thomas et al., 2016). Alternate explanations for the observed trend are increasing light-use efficiency because of CO_2 fertilization (Bastos et al., 2019; Piao et al., 2017; Thomas et al., 2016; Wenzel et al., 2016) or high-latitude warming effects on biome distribution and plant productivity (Forkel et al., 2016). Warming effects emerged as important in simulations using the LPJmL TBM which accurately simulates the large observed ASC trend, (Forkel et al., 2016), but simulates a global GPP trend ($PgC/year^2$; 1970–2011; Forkel et al., 2016) that is less than half the corresponding CABLE-simulated trend (0.53 ± 0.02 $PgC/year^2$; 1970–2011). The CABLE trend is compatible with the COS-based estimate (Campbell et al., 2017), whereas the LPJmL estimate appears too low. LPJmL is thus an example of a model that satisfies the regional ASC constraint, but not the global constraint on the trend in GPP. The high-CO_2 fertilization effect in CABLE, which is dominated by a leaf-level effect in the Northern Hemisphere (Figure 4b,d), supports the hypothesis of increasing light-use efficiency as a key driver of the amplitude of seasonal cycle increase. However, we note that this increase is highly dependent on lags between photosynthesis and ecosystem respiration and cannot be readily disentangled into warming versus c_a-driven trends in GPP.

The uncertain contribution of agricultural intensification to the increase in seasonal amplitude of CO_2 in the Northern Hemisphere has been the subject of much debate (Gray et al., 2014; MacBean & Peylin, 2014; Zeng et al., 2014), but the following four points argue against agricultural intensification being a major contributor to global GPP increase: (a) the seasonal amplitude of CO_2 in the Northern Hemisphere is sensitive to CO_2 uptake and release north of 35°N

(Graven et al., 2013) and not the whole globe, and land north of 35°N contributes less than 25% to global GPP (Figure S9). (b) Globally, it has been estimated that the combined effects of land use change and land management over the last century—including expansion of agricultural lands, and intensification by irrigation and fertilization—have had almost no impact on global NPP (Bondeau et al., 2007, figure 15f), although the effects on the seasonal cycle are nontrivial (Calle, Poulter, & Patra, 2019). (c) Expansion of agricultural land area over the last century has been dominated by clearing of tropical forest—a land use conversion that is expected to contribute negatively to trends in NPP (Nyawira et al., 2016). (d) Recent studies using multiple models and data sets have concluded that the effect of land use change and land management on the increase in seasonal amplitude of CO_2 in the Northern Hemisphere is very small compared with the effects of CO_2 fertilization and warming-induced lengthening of growing season (Bastos et al., 2019; Piao et al., 2017). Bastos et al. (2019) identify Eurasia as the region contributing most to increasing seasonal amplitude of CO_2—a region that is dominated by natural ecosystems and has experienced very little land use change (Verburg et al., 2015) over the last half-century. A limitation of the study by Piao et al. (2017) is that it relies on an ensemble of models, many of which do not account for agricultural intensification. Bastos et al. (2019) address this limitation in their more recent study, by complementing the ecosystem model results with trend driver attribution using statistical models, confirming that the observed trends in seasonal amplitude of CO_2 are not significantly related to agricultural intensification.

By reconciling multiple global-scale observational constraints, we identified a CO_2 fertilization effect on historical global GPP that is significantly higher than current estimates. Independent regional studies using amplitude of seasonal cycle data (Northern Hemisphere extra-tropics; Wenzel et al., 2016) and catchment water balance (tropical forests; Yang et al., 2016) have also inferred larger CO_2 fertilization effects than predicted by TBM ensembles. The causes of such model-data discrepancies are poorly known, but biases associated with the representation of nutrient limitations on GPP have been invoked as one possible cause (Wenzel et al., 2016; Yang et al., 2016). Our results, that account for nitrogen-cycle effects on ecosystem productivity, suggest that underprediction of GPP trends and CO_2 responses is associated with a failure by current TBMs to account for plant coordination of photosynthesis. This finding is important for the future role of land carbon sinks, suggesting an underestimate by current models of potential CO_2 removal under low-emission scenarios consistent with the Paris Agreement targets.

ACKNOWLEDGEMENTS

We thank the TRENDY modellers: Stephen Sitch, Peter Anthoni, Vivek Arora, Atul Jain, Joe Melton, Benjamin Poulter, Benjamin Stocker, Hanqin Tian, Anthony Walker, Andy Wiltshire, Sönke Zaehle, Nicolas Viovy, Ning Zeng, and Dan Zhu for access to the TRENDYv6 simulations of GPP and the NLS. We also thank the HIPPO science team, who collected the aircraft c_a measurements. VH, JGC, PRB, and CMT acknowledge the support from the Earth Systems and Climate Change Hub, funded by the Australian Government's National Environmental Science Program. BS contributions to this work were supported by the Strategic Research Area MERGE and by a CSIRO Distinguished Visiting Scientist grant. MC was supported by a grant overseen by the French National Research Agency (ANR) as part of the "Investissements d'Avenir" program (ANR-11-LABX-0002-01, Lab of Excellence ARBRE). SM-F's contributions were supported by NIWA core funding through the Greenhouse Gases, Emissions and Carbon Cycle Science Programme.

DATA AVAILABILITY STATEMENT

CABLE simulations used in this study can be found at: https://doi.org/10.5281/zenodo.3629955. The CABLE source code can be accessed after registration at https://trac.nci.org.au/trac/cable. Simulations in this work used Revision Number 4546.

ORCID

Vanessa Haverd https://orcid.org/0000-0003-4359-5895
Benjamin Smith https://orcid.org/0000-0002-6987-5337
Josep G. Canadell https://orcid.org/0000-0002-8788-3218
Matthias Cuntz https://orcid.org/0000-0002-5966-1829
Sara Mikaloff-Fletcher https://orcid.org/0000-0003-0741-0320
Graham Farquhar https://orcid.org/0000-0002-7065-1971
William Woodgate https://orcid.org/0000-0001-8945-5105
Peter R. Briggs https://orcid.org/0000-0002-7164-0545
Cathy M. Trudinger https://orcid.org/0000-0002-4844-2153

REFERENCES

Ahlstrom, A., Raupach, M. R., Schurgers, G., Smith, B., Arneth, A., Jung, M., … Zeng, N. (2015). The dominant role of semi-arid ecosystems in the trend and variability of the land CO_2 sink. *Science*, *348*, 895–899. https://doi.org/10.1126/science.aaa1668

Ainsworth, E. A., & Rogers, A. (2007). The response of photosynthesis and stomatal conductance to rising [CO_2]: Mechanisms and environmental interactions. *Plant, Cell & Environment*, *30*, 258–270.

Ali, A. A., Xu, C., Rogers, A., Fisher, R. A., Wullschleger, S. D., Massoud, E. C., … Wilson, C. J. (2016). A global scale mechanistic model of photosynthetic capacity (LUNA V1.0). *Geoscientific Model Development*, *9*, 587–606. https://doi.org/10.5194/gmd-9-587-2016

Bahar, N. H. A., Hayes, L., Scafaro, A. P., Atkin, O. K., & Evans, J. R. (2018). Mesophyll conductance does not contribute to greater photosynthetic rate per unit nitrogen in temperate compared with tropical evergreen wet-forest tree leaves. *New Phytologist*, *218*, 492–505. https://doi.org/10.1111/nph.15031

Baldocchi, D., Ryu, Y., & Keenan, T. (2016). Terrestrial carbon cycle variability. *F1000Research*, *5*, 2371. https://doi.org/10.12688/f1000research.8962.1

Bastos, A., Ciais, P., Chevallier, F., Rödenbeck, C., Ballantyne, A. P., Maignan, F., … Zhu, D. (2019). Contrasting effects of CO_2 fertilisation, land-use change and warming on seasonal amplitude of northern hemisphere CO_2 exchange. *Atmospheric Chemistry and Physics*, *19*, 12361–12375. https://doi.org/10.5194/acp-19-12361-2019

Bondeau, A., Smith, P. C., Zaehle, S., Schaphoff, S., Lucht, W., Cramer, W., … Smith, B. (2007). Modelling the role of agriculture for the 20th century global terrestrial carbon balance. *Global Change Biology*, *13*, 679–706. https://doi.org/10.1111/j.1365-2486.2006.01305.x

Calle, L., Poulter, B., & Patra, P. K. (2019). A segmentation algorithm for characterizing rise and fall segments in seasonal cycles: An

application to XCO_2 to estimate benchmarks and assess model bias. *Atmospheric Measurement Techniques*, *12*, 2611–2629. https://doi.org/10.5194/amt-12-2611-2019

Campbell, J. E., Berry, J. A., Seibt, U., Smith, S. J., Montzka, S. A., Launois, T., … Laine, M. (2017). Large historical growth in global terrestrial gross primary production. *Nature*, *544*, 84–87. https://doi.org/10.1038/nature22030

Chang, J., Ciais, P., Wang, X., Piao, S., Asrar, G., Betts, R., … Zhao, F. (2017). Benchmarking carbon fluxes of the ISIMIP2a biome models. *Environmental Research Letters*, *12*, 045002. https://doi.org/10.1088/1748-9326/aa63fa

Chen, J.-L., Reynolds, J. F., Harley, P. C., & Tenhunen, J. D. (1993). Coordination theory of leaf nitrogen distribution in a canopy. *Oecologia*, *93*, 63–69. https://doi.org/10.1007/BF00321192

Ciais, P., Sabine, C., Bala, G., Bopp, L., Brovkin, V., Canadell, J., … Thornton, P. (2013). Carbon and other biogeochemical cycles. In T. F. Stocker, D. Qin, G.-K. Plattner, M. Tignor, S. K. Allen, J. Boschung, A. Nauels, Y. Xia, V. Bex, & P. M. Midgley (Eds.), *Climate change 2013: The physical science basis. Contribution of working group I to the fifth assessment report of the Intergovernmental Panel on Climate Change* (pp. 465–570). Cambridge, UK and New York, NY: Cambridge University Press.

De Kauwe, M. G., Keenan, T. F., Medlyn, B. E., Prentice, I. C., & Terrer, C. (2016). Satellite based estimates underestimate the effect of CO_2 fertilization on net primary productivity. *Nature Climate Change*, *6*, 892–893. https://doi.org/10.1038/nclimate3105

Dlugokencky, E., & Tans, P. (2017). Trends in atmospheric carbon dioxide, National Oceanic & Atmospheric Administration, Earth System Research Laboratory (NOAA/ESRL). Retrieved from http://www.esrl.noaa.gov/gmd/ccgg/trends/global.html

Donohue, R. J., Roderick, M. L., Mcvicar, T. R., & Farquhar, G. D. (2013). Impact of CO_2 fertilization on maximum foliage cover across the globe's warm, arid environments. *Geophysical Research Letters*, *40*, 3031–3035.

Ellsworth, D. S., Anderson, I. C., Crous, K. Y., Cooke, J., Drake, J. E., Gherlenda, A. N., … Reich, P. B. (2017). Elevated CO_2 does not increase eucalypt forest productivity on a low-phosphorus soil. *Nature Climate Change*, *7*, 279. https://doi.org/10.1038/nclimate3235

Farquhar, G. V., Caemmerer, S. V., & Berry, J. (1980). A biochemical model of photosynthetic CO_2 assimilation in leaves of C3 species. *Planta*, *149*, 78–90. https://doi.org/10.1007/BF00386231

Farquhar, G. D., & Von Caemmerer, S. (1981). Some relationships between the biochemistry of photosynthesis and the gas exchange of leaves. *Planta*, *153*, 376–387. https://doi.org/10.1007/BF00384257

Forkel, M., Carvalhais, N., Rodenbeck, C., Keeling, R., Heimann, M., Thonicke, K., … Reichstein, M. (2016). Enhanced seasonal CO_2 exchange caused by amplified plant productivity in northern ecosystems. *Science*, *351*(6274), 696–699. https://doi.org/10.1126/science.aac4971

Forzieri, G., Alkama, R., Miralles, D. G., & Cescatti, A. (2017). Satellites reveal contrasting responses of regional climate to the widespread greening of Earth. *Science*, *356*, 1180–1184. https://doi.org/10.1126/science.aal1727

Franks, P. J., Adams, M. A., Amthor, J. S., Barbour, M. M., Berry, J. A., Ellsworth, D. S., … von Caemmerer, S. (2013). Sensitivity of plants to changing atmospheric CO_2 concentration: From the geological past to the next century. *New Phytologist*, *197*, 1077–1094. https://doi.org/10.1111/nph.12104

Graven, H. D., Keeling, R. F., Piper, S. C., Patra, P. K., Stephens, B. B., Wofsy, S. C., … Bent, J. D. (2013). Enhanced seasonal exchange of CO_2 by northern ecosystems since 1960. *Science*, *341*, 1085–1089. https://doi.org/10.1126/science.1239207

Gray, J. M., Frolking, S., Kort, E. A., Ray, D. K., Kucharik, C. J., Ramankutty, N., & Friedl, M. A. (2014). Direct human influence on atmospheric CO_2 seasonality from increased cropland productivity. *Nature*, *515*, 398–401. https://doi.org/10.1038/nature13957

Haverd, V., Cuntz, M., Nieradzik, L. P., & Harman, I. N. (2016). Improved representations of coupled soil–canopy processes in the CABLE land surface model (Subversion revision 3432). *Geoscientific Model Development*, *9*, 3111–3122. https://doi.org/10.5194/gmd-9-3111-2016

Haverd, V., Raupach, M. R., Briggs, P. R., Canadell, J. G., Isaac, P., Pickett-Heaps, C., … Wang, Z. (2013). Multiple observation types reduce uncertainty in Australia's terrestrial carbon and water cycles. *Biogeosciences*, *10*, 2011–2040. https://doi.org/10.5194/bg-10-2011-2013

Haverd, V., Smith, B., Cook, G. D., Briggs, P. R., Nieradzik, L., Roxburgh, S. H., … Canadell, J. G. (2013). A stand-alone tree demography and landscape structure module for Earth system models. *Geophysical Research Letters*, *40*, 5234–5239. https://doi.org/10.1002/grl.50972

Haverd, V., Smith, B., Nieradzik, L., Briggs, P. R., Woodgate, W., Trudinger, C. M., … Cuntz, M. (2018). A new version of the CABLE land surface model (Subversion revision r4601) incorporating land use and land cover change, woody vegetation demography, and a novel optimisation-based approach to plant coordination of photosynthesis. *Geoscientific Model Development*, *11*, 2995–3026. https://doi.org/10.5194/gmd-11-2995-2018

Heimann, M., & Körner, S. (2005). The global atmospheric tracer model TM3. In S. Körner (Ed.), *Technical Reports* (pp. 1–131). Jena, Germany: Max-Planck-Institut für Biogeochemie.

Hickler, T., Smith, B., Prentice, I. C., Mjofors, K., Miller, P., Arneth, A., & Sykes, M. T. (2008). CO_2 fertilization in temperate FACE experiments not representative of boreal and tropical forests. *Global Change Biology*, *14*, 1531–1542. https://doi.org/10.1111/j.1365-2486.2008.01598.x

Houghton, R. A., & Nassikas, A. A. (2018). Negative emissions from stopping deforestation and forest degradation, globally. *Global Change Biology*, *24*, 350–359. https://doi.org/10.1111/gcb.13876

Hurtt, G. C., Chini, L. P., Frolking, S., Betts, R. A., Feddema, J., Fischer, G., … Wang, Y. P. (2011). Harmonization of land-use scenarios for the period 1500–2100: 600 years of global gridded annual land-use transitions, wood harvest, and resulting secondary lands. *Climatic Change*, *109*, 117–161. https://doi.org/10.1007/s10584-011-0153-2

Hurtt, G., Chini, L., Frolking, S., & Sahajpal, R. (2016). Land use harmonisation 2 (LUH2) v2h. Retrieved from http://luh.umd.edu/data.shtml

Hurtt, G., Chini, L., Frolking, S., & Sahajpal, R. (2018). Land use harmonisation 2 (LUH2) v2f SSP1 RCP2.6 (from IMAGE). Retrieved from http://luh.umd.edu/data.shtml

Jung, M., Reichstein, M., Margolis, H. A., Cescatti, A., Richardson, A. D., Arain, M. A., … Williams, C. (2011). Global patterns of land-atmosphere fluxes of carbon dioxide, latent heat, and sensible heat derived from eddy covariance, satellite, and meteorological observations. *Journal of Geophysical Research: Biogeosciences*, *116*, https://doi.org/10.1029/2010JG001566

Kalnay, E., Kanamitsu, M., Kistler, R., Collins, W., Deaven, D., Gandin, L., … Joseph, D. (1996). The NCEP/NCAR 40-year reanalysis project. *Bulletin of the American Meteorological Society*, *77*, 437–472. https://doi.org/10.1175/1520-0477(1996)077<0437:TNYRP>2.0.CO;2

Keeling, C. D., Harris, T. B., & Wilkins, E. M. (1968). Concentration of atmospheric carbon dioxide at 500 and 700 millibars. *Journal of Geophysical Research*, *73*, 4511–4528. https://doi.org/10.1029/JB073i014p04511

Keeling, C. D., Piper, S. C., Bacastow, R. B., Wahlen, M., Whorf, T. P., Heimann, M., & Meijer, H. A. (2001). *Exchanges of atmospheric CO_2 and $^{13}CO_2$ with the terrestrial biosphere and oceans from 1978 to 2000. I. Global aspects* (pp. 1–28). UC San Diego: Scripps Institution of Oceanography. Retrieved from https://escholarship.org/uc/item/09v319r9

Keenan, T. F., Prentice, I. C., Canadell, J. G., Williams, C. A., Wang, H., Raupach, M., & Collatz, G. J. (2016). Recent pause in the growth

rate of atmospheric CO_2 due to enhanced terrestrial carbon uptake. *Nature Communications*, *7*, 13428. https://doi.org/10.1038/ncomms13428

Kooijmans, L. M. J., Sun, W. U., Aalto, J., Erkkilä, K.-M., Maseyk, K., Seibt, U., … Chen, H. (2019). Influences of light and humidity on carbonyl sulfide-based estimates of photosynthesis. *Proceedings of the National Academy of Sciences*, *116*, 2470–2475. https://doi.org/10.1073/pnas.1807600116

Koven, C. D., Riley, W. J., Subin, Z. M., Tang, J. Y., Torn, M. S., Collins, W. D., … Swenson, S. C. (2013). The effect of vertically resolved soil biogeochemistry and alternate soil C and N models on C dynamics of CLM4. *Biogeosciences*, *10*, 7109–7131. https://doi.org/10.5194/bg-10-7109-2013

Kowalczyk, E., Stevens, L., Law, R., Dix, M., Wang, Y., Harman, I., … Ziehn, T. (2013). The land surface model component of ACCESS: Description and impact on the simulated surface climatology. *Australian Meteorological and Oceanographic Journal*, *63*, 65–82. https://doi.org/10.22499/2.6301.005

Lamarque, J.-F., Kyle, G. P., Meinshausen, M., Riahi, K., Smith, S. J., van Vuuren, D. P., … Vitt, F. (2011). Global and regional evolution of short-lived radiatively-active gases and aerosols in the Representative Concentration Pathways. *Climatic Change*, *109*, 191–212. https://doi.org/10.1007/s10584-011-0155-0

Le Quéré, C., Andrew, R. M., Friedlingstein, P., Sitch, S., Pongratz, J., Manning, A. C., … Zhu, D. (2018). Global carbon budget 2017. *Earth System Science Data*, *10*, 405–448. https://doi.org/10.5194/essd-10-405-2018

Li, W., Ciais, P., Wang, Y., Yin, Y. I., Peng, S., Zhu, Z., … Piao, S. (2018). Recent changes in global photosynthesis and terrestrial ecosystem respiration constrained from multiple observations. *Geophysical Research Letters*, *45*, 1058–1068. https://doi.org/10.1002/2017GL076622

Liptak, J., Keppel-Aleks, G., & Lindsay, K. (2017). Drivers of multi-century trends in the atmospheric CO_2 mean annual cycle in a prognostic ESM. *Biogeosciences*, *14*, 1383–1401.

Lloyd, J., & Farquhar, G. D. (1996). The CO_2 dependence of photosynthesis, plant growth responses to elevated atmospheric co_2 concentrations and their interaction with soil nutrient status. I. General principles and forest ecosystems. *Functional Ecology*, *10*, 4–32.

Long, S. P. (1991). Modification of the response of photosynthetic productivity to rising temperature by atmospheric CO_2 concentrations: Has its importance been underestimated? *Plant, Cell & Environment*, *14*, 729–739. https://doi.org/10.1111/j.1365-3040.1991.tb01439.x

Macbean, N., & Peylin, P. (2014). Agriculture and the global carbon cycle. *Nature*, *515*, 351. https://doi.org/10.1038/515351a

Maire, V., Martre, P., Kattge, J., Gastal, F., Esser, G., Fontaine, S., & Soussana, J.-F. (2012). The coordination of leaf photosynthesis links C and N fluxes in C_3 plant species. *PLoS ONE*, *7*, e38345. https://doi.org/10.1371/journal.pone.0038345

McGuire, A. D., Lawrence, D. M., Koven, C., Clein, J. S., Burke, E., Chen, G., … Zhuang, Q. (2018). Dependence of the evolution of carbon dynamics in the northern permafrost region on the trajectory of climate change. *Proceedings of the National Academy of Sciences of the United States of America*, *115*, 3882–3887. https://doi.org/10.1073/pnas.1719903115

Mueller, T., Dressler, G., Tucker, C., Pinzon, J., Leimgruber, P., Dubayah, R., … Fagan, W. (2014). Human land-use practices lead to global long-term increases in photosynthetic capacity. *Remote Sensing*, *6*, 5717–5731. https://doi.org/10.3390/rs6065717

Norby, R. J., Delucia, E. H., Gielen, B., Calfapietra, C., Giardina, C. P., King, J. S., … Oren, R. (2005). Forest response to elevated CO_2 is conserved across a broad range of productivity. *Proceedings of the National Academy of Sciences of the United States of America*, *102*, 18052–18056. https://doi.org/10.1073/pnas.0509478102

Nyawira, S. S., Nabel, J. E. M. S., Don, A., Brovkin, V., & Pongratz, J. (2016). Soil carbon response to land-use change: Evaluation of a global vegetation model using observational meta-analyses. *Biogeosciences*, *13*, 5661–5675. https://doi.org/10.5194/bg-13-5661-2016

O'Neill, B. C., Kriegler, E., Ebi, K. L., Kemp-Benedict, E., Riahi, K., Rothman, D. S., … Solecki, W. (2017). The roads ahead: Narratives for shared socioeconomic pathways describing world futures in the 21st century. *Global Environmental Change*, *42*, 169–180. https://doi.org/10.1016/j.gloenvcha.2015.01.004

Parazoo, N. C., Commane, R., Wofsy, S. C., Koven, C. D., Sweeney, C., Lawrence, D. M., … Miller, C. E. (2016). Detecting regional patterns of changing CO_2 flux in Alaska. *Proceedings of the National Academy of Sciences of the United States of America*, *113*, 7733–7738. https://doi.org/10.1073/pnas.1601085113

Piao, S., Liu, Z., Wang, Y., Ciais, P., Yao, Y., Peng, S., … Wang, T. (2017). On the causes of trends in the seasonal amplitude of atmospheric CO_2. *Global Change Biology*, *24*, 608–618. https://doi.org/10.1111/gcb.13909

Piao, S., Sitch, S., Ciais, P., Friedlingstein, P., Peylin, P., Wang, X., … Zeng, N. (2013). Evaluation of terrestrial carbon cycle models for their response to climate variability and to CO_2 trends. *Global Change Biology*, *19*, 2117–2132. https://doi.org/10.1111/gcb.12187

Schimel, D., Stephens, B. B., & Fisher, J. B. (2015). Effect of increasing CO_2 on the terrestrial carbon cycle. *Proceedings of the National Academy of Sciences of the United States of America*, *112*, 436–441.

Sitch, S., Friedlingstein, P., Gruber, N., Jones, S. D., Murray-Tortarolo, G., Ahlström, A., … Myneni, R. (2015). Recent trends and drivers of regional sources and sinks of carbon dioxide. *Biogeosciences*, *12*, 653–679. https://doi.org/10.5194/bg-12-653-2015

Still, C. J., Berry, J. A., Collatz, G. J., & Defries, R. S. (2003). Global distribution of C_3 and C_4 vegetation: Carbon cycle implications. *Global Biogeochemical Cycles*, *17*, 6-1-6-14.

Pugh, T., Müller, C., Arneth, A., Haverd, V., & Smith, B. (2016). Key knowledge and data gaps in modelling the influence of CO_2 concentration on the terrestrial carbon sink. *Journal of Plant Physiology*, *203*, 3–15. https://doi.org/10.1016/j.jplph.2016.05.001

Thomas, R. T., Prentice, I. C., Graven, H., Ciais, P., Fisher, J. B., Hayes, D. J., … Zeng, N. (2016). Increased light-use efficiency in northern terrestrial ecosystems indicated by CO_2 and greening observations. *Geophysical Research Letters*, *43*, 11,339–311,349. https://doi.org/10.1002/2016GL070710

Thornley, J. H. M. (2004). Acclimation of photosynthesis to light and canopy nitrogen distribution: An interpretation. *Annals of Botany*, *93*, 473–475. https://doi.org/10.1093/aob/mch051

van Vuuren, D. P., Edmonds, J., Kainuma, M., Riahi, K., Thomson, A., Hibbard, K., … Rose, S. K. (2011). The representative concentration pathways: An overview. *Climatic Change*, *109*, 5–31. https://doi.org/10.1007/s10584-011-0148-z

Verburg, P. H., Crossman, N., Ellis, E. C., Heinimann, A., Hostert, P., Mertz, O., … Zhen, L. (2015). Land system science and sustainable development of the earth system: A global land project perspective. *Anthropocene*, *12*, 29–41. https://doi.org/10.1016/j.ancene.2015.09.004

Viovy, N. (2009). CRU-NCEP CRUNCEP version 7 – Atmospheric forcing data for the community land model. Research Data Archive at the National Center for Atmospheric Research, Computational and Information Systems Laboratory. Dataset. Retrieved from http://rda.ucar.edu/datasets/ds314.3/

Walker, A. P., Beckerman, A. P., Gu, L., Kattge, J., Cernusak, L. A., Domingues, T. F., … Ian Woodward, F. (2014). The relationship of leaf photosynthetic traits – V_{cmax} and J_{max} – To leaf nitrogen, leaf phosphorus, and specific leaf area: A meta-analysis and modeling study. *Ecology and Evolution*, *4*, 3218–3235. https://doi.org/10.1002/ece3.1173

Wang, H., Prentice, I. C., Keenan, T. F., Davis, T. W., Wright, I. J., Cornwell, W. K., … Peng, C. (2017). Towards a universal model for carbon dioxide uptake by plants. *Nature Plants*, *3*, 734–741. https://doi.org/10.1038/s41477-017-0006-8

Wang, Y. P., Kowalczyk, E., Leuning, R., Abramowitz, G., Raupach, M. R., Pak, B., … Luhar, A. (2011). Diagnosing errors in a land surface model (CABLE) in the time and frequency domains. *Journal of Geophysical Research*, *116*. https://doi.org/10.1029/2010JG001385

Wang, Y. P., Law, R. M., & Pak, B. (2010). A global model of carbon, nitrogen and phosphorus cycles for the terrestrial biosphere. *Biogeosciences*, *7*, 2261–2282. https://doi.org/10.5194/bg-7-2261-2010

Warszawski, L., Frieler, K., Huber, V., Piontek, F., Serdeczny, O., & Schewe, J. (2014). The Inter-Sectoral Impact Model Intercomparison Project (ISI–MIP): Project framework. *Proceedings of the National Academy of Sciences of the United States of America*, *111*, 3228–3232. https://doi.org/10.1073/pnas.1312330110

Wenzel, S., Cox, P. M., Eyring, V., & Friedlingstein, P. (2016). Projected land photosynthesis constrained by changes in the seasonal cycle of atmospheric CO_2. *Nature*, *538*, 499–501. https://doi.org/10.1038/nature19772

Whelan, M. E., Lennartz, S. T., Gimeno, T. E., Wehr, R., Wohlfahrt, G., Wang, Y., … Campbell, J. E. (2018). Reviews and syntheses: Carbonyl sulfide as a multi-scale tracer for carbon and water cycles. *Biogeosciences*, *15*, 3625–3657. https://doi.org/10.5194/bg-15-3625-2018

Wofsy, S. C. (2011). HIAPER Pole-to-Pole Observations (HIPPO): Fine-grained, global-scale measurements of climatically important atmospheric gases and aerosols. *Philosophical Transactions of the Royal Society A: Mathematical, Physical and Engineering Sciences*, *369*, 2073–2086. https://doi.org/10.1098/rsta.2010.0313

Wong, S. C. (1979). Elevated atmospheric partial pressure of CO_2 and plant growth. I. Interactions of nitrogen nutrition and photosynthetic capacity in C_3 and C_4 plants. *Oecologia*, *44*, 68–74.

Yang, Y., Donohue, R. J., Mcvicar, T. R., Roderick, M. L., & Beck, H. E. (2016). Long-term CO_2 fertilization increases vegetation productivity and has little effect on hydrological partitioning in tropical rainforests. *Journal of Geophysical Research: Biogeosciences*, *121*, 2125–2140.

Zaehle, S., Medlyn, B. E., De Kauwe, M. G., Walker, A. P., Dietze, M. C., Hickler, T., … Norby, R. J. (2014). Evaluation of 11 terrestrial carbon–nitrogen cycle models against observations from two temperate Free-Air CO_2 Enrichment studies. *New Phytologist*, *202*, 803–822. https://doi.org/10.1111/nph.12697

Zeng, N., Zhao, F., Collatz, G. J., Kalnay, E., Salawitch, R. J., West, T. O., & Guanter, L. (2014). Agricultural Green Revolution as a driver of increasing atmospheric CO_2 seasonal amplitude. *Nature*, *515*, 394–397. https://doi.org/10.1038/nature13893

Zhu, Z., Piao, S., Myneni, R. B., Huang, M., Zeng, Z., Canadell, J. G., … Zeng, N. (2016). Greening of the Earth and its drivers. *Nature Climate Change*, *6*(8), 791–795. https://doi.org/10.1038/nclimate3004

SUPPORTING INFORMATION

Additional supporting information may be found online in the Supporting Information section.

How to cite this article: Haverd V, Smith B, Canadell JG, et al. Higher than expected CO_2 fertilization inferred from leaf to global observations. *Glob Change Biol*. 2020;26:2390–2402. https://doi.org/10.1111/gcb.14950